JOURNAL OF AIR TRANSPORTATION
Vol. 31, No. 4, October–December 2023

Predeparture Flight Planning to Minimize Operating Cost for Urban Air Mobility

Hualong Tang,* Yu Zhang,† and Joseph Post‡
University of South Florida, Tampa, Florida 33620

https://doi.org/10.2514/1.D0332

Urban air mobility (UAM) is envisioned to move to highly automated and high-density operations in low-altitude urban airspace in the future. Providers of services for UAM (PSU), rather than the legacy air traffic control, are anticipated to support operators with operational planning, aircraft deconfliction, conformance monitoring, and emergency information dissemination. Such services, for hundreds to thousands of simultaneous UAM operations in constrained airspace, can only be realized with automated systems. In this study, airspace and deconfliction models for generating predeparture conflict-free four-dimensional (4-D) flight trajectories are proposed, which can be further developed into an automated flight planning tool for PSU. A semistructured scalable airspace design for future UAM is proposed (i.e., a layered airspace topology with direct routes between vertiports, avoiding physical obstacles, such as buildings, obstructions, and restricted airspace) using the visibility graph method. Based on the proposed airspace design, deconfliction strategies (e.g., flight-level assignment and departure delay) are applied to obtain predeparture conflict-free 4-D trajectories of UAM operations by solving a mixed-integer programming problem, with the objective function to minimize the operating cost of UAM operations. Furthermore, sensitivity analysis is performed to investigate the impacts of three key cost parameters (electricity price, crew hourly rate, and maintenance hourly rate). The relationships of departure delay bound (maximum departure delay allowed) vs operating cost saving and departure delay bound vs delay cost to passengers are examined, as is the tradeoff between operating cost saving and passenger delay cost.

I. Introduction

URBAN air mobility (UAM) is anticipated to evolve from the initial stage of low-density and low-complexity operations, such as air shuttles, to a mature stage of highly automated and high-density and -complexity on-demand operations with hundreds to thousands of simultaneous operations in the urban airspace [1]. The order-of-magnitude increase in operations plus the unique low-altitude operating environment, where aircraft need to conform to constraints, such as buildings, obstructions, and restricted airspace, demand a new sector [providers of services for UAM (PSU)] that has to be supported by an automated traffic management system. Such a system needs to answer two critical questions for predeparture flight planning:

1) How should airspace be structured?
2) How should conflicts be resolved?

There has been a debate between unstructured airspace vs structured airspace regarding the capacity, safety, and efficiency of the airspace. Some studies found that structured airspace can greatly reduce airspace complexity and simplify conflict detection and separation assurance, and thus lessen Air Traffic Control workload [2,3]. On the other hand, some researchers argue that a lightly structured architecture, especially free flight, spreads traffic over the airspace to reduce the number of potential conflicts, and flights can fly their most economic routes to save fuel [4,5].

Structured airspace topology inspired by roadway design, for example, has been proposed in several studies for unmanned aircraft system (UAS)/UAM [6–9]. Unstructured airspace topology is mostly seen in a distributed system with free flight for UAM [9]. The airspace topology proposed by Geister and Korn [10] lies between structured and unstructured, as the airspace is separated into different regions by geofence; inside each region, aircraft can perform free flight. The layered airspace topology discretized the airspace into grids to generate flight routes at each layer that are approximations of shortest paths [11,12], whereas Tang et al. [13] constructed flight routes based on the obstacle vertices at each layer with minimal nodes and edges, and the routes generated are actual shortest paths.

The performance of UAM/UAS operations in terms of safety, efficiency, and capacity is directly influenced by the characteristics of the airspace structure. Various airspace concepts have been proposed for UAM/UAS operations, each with its advantages and limitations. The Federal Aviation Administration's (FAA) corridor airspace concept confines UAM operations to a designated space, which separates them from other operations and enhances safety [9]. However, this concept may limit network efficiency due to the restricted point-to-point operations. Jang et al. [7] divided the urban airspace into multiple layers above a street, with three types of airspace structures from most to least restrictive. Restrictive structures offer better safety but reduce capacity, whereas less restrictive structures are more efficient but may compromise safety. U-space's airspace concept for drone operations partitions the low-altitude airspace into three zones (types X, Y, and Z) based on different requirements. Although this concept provides flexibility in accommodating different types of operations, it may result in lower safety and capacity performance than a layered design. To achieve a balanced performance in capacity, safety, and efficiency, the simulation conducted by Sunil et al. [14] demonstrated that a layered concept with minimal structure at each layer could be optimal.

To address the challenge of medium- to high-density operations, such as a UAM maturity level of 4 and above (i.e., hundreds to thousands of simultaneous operations in a metropolitan area with high automation reliance [1]), both the FAA and Single European Sky ATM Research UAM/UAS concept of operations envision deconfliction being a shared responsibility of onboard vehicle automation capabilities, mainly providing tactical detect and avoid, whereas PSU provides strategic traffic management [8,15]. Most tactical deconfliction methods for UAM/UAS apply a distributed approach under the concept of free flight, assuming aircraft can freely fly in a defined volume as long as they avoid obstacles and restricted areas. They are typically confined to smaller airspace (i.e., sectors) to solve conflicts in real time as opposed to strategic deconfliction that targets network scales in the planning phase. Those methods include techniques inspired by physical laws, geometric optimization, and the Markov

Presented as Paper 2022-3318 at the AIAA Aviation 2022 Forum, Chicago, IL, June 27–July 1, 2022; received 13 July 2022; revision received 1 April 2023; accepted for publication 4 April 2023; published online 18 May 2023.

*Graduate Research Assistant, Civil and Environmental Engineering.
†Professor, Civil and Environmental Engineering.
‡Senior Research Associate, Civil and Environmental Engineering. Senior Member AIAA.

decision process (MDP) [16–18]. One of the main issues with distributed approaches is that the global optimum is not always guaranteed. Loss of separation (LOS) was observed to occur at the rate of 1 per 100 flight hours in Yang and Wei [18]. For strategically (i.e., predeparture) conflict detection and resolution, centralized approaches typically have been used by implementing strategies, such as flight-level change, departure time delay, and speed control. Zhu and Wei [16] proposed a linear programming model to plan predeparture conflict-free trajectories on a structured single cruise level with conflict resolutions through rerouting and delaying departure time. Tang et al. [13] proposed an integer programming model to deconflict flight paths by applying flight-level assignment (FLA) on layered airspace and a multiplication model (formulated as a second-order cone program) to ensure fairness among different operators. Besides centralized approaches, Bertram et al. [9] proposed a distributed approach in strategic deconfliction, where the authors modeled strategic deconfliction as an MDP and solved it with FastMDP to generate conflict-free trajectories. The issue with distributed approaches, such as MDP, applied to strategic deconfliction is the airspace availability when planning flights in large-scale airspace. Only 28% of the airspace is available (excluding controlled airspace and special use airspace) for UAM operations at 1500 ft in the San Francisco Bay area [19]. Having less volume of airspace for aircraft to maneuver, particularly in departure and arrival airspace with higher flight densities, could dramatically degrade the performance of distributed approaches in strategic deconfliction.

This study aimed to develop a scalable airspace model and automated strategic deconfliction approaches to support predeparture flight planning services for medium- to high-density UAM operations (hundreds of and above simultaneous operations in a metropolitan area) that could be employed by PSU. We adopted the layered airspace topology with free flight at each layer from Tang et al. [13] given that it maintains the best balance between airspace capacity, efficiency, and safety and uses minimal nodes and edges to build the scalable route network. When constructing the en route network, only the conflicting points between different routes were considered in Tang et al. [13]. However, conflicts could also happen at the same entry or exit point of two routes. This study further considered the conflicts at the en route entry/exit points, which largely increases the number of potential conflicts that need to be taken into account. We assumed there will be tactical departure and arrival management taking care of operations connecting the vertiport and en route airspace; thus, the departure and approach procedures and the conflicts between these procedures and en route paths were outside the scope of this paper. We assumed that UAM flight will be conducted within controlled airspace, and that the routes for these flights should be designed in a way that ensures physical or procedural separation from existing routes. As a result, any potential conflicts arising from interactions between UAM and existing air traffic are beyond the scope of this paper.

To ensure predeparture conflict-free flight, we applied strategic approaches [FLA plus departure delay (DD)] to deconflict aircraft, which adds another degree of freedom to the strategies applied in Tang et al. [13]. A mixed-integer linear programming (MILP) model is proposed to minimize the operating cost of UAM operations. A rolling-window algorithm is developed to solve the problem sequentially. We conducted experiments to investigate the sensitivity of operating cost to three key cost parameters (electricity price, crew hourly rate, and maintenance hourly rate). The relationships of DD bound vs operating cost savings and DD bound vs delay cost to passengers are examined, as is the tradeoff between operating cost saving and passenger delay cost.

II. Methodology

A. Airspace Structure

The airspace construct process is based on the low-altitude airspace management system proposed in Tang et al. [13]. The airspace is configured with several layers, and an aircraft can freely fly on that layer except for areas that are restricted or occupied by buildings, obstacles, or obstructions. We first constructed a three-dimensional (3-D) Geographic Information System (GIS) map, which provides the available airspace that can be used by UAM flights. Then, the visibility graph method was used to generate candidate flight routes connecting any pair of en route entry and exit points on each cruise level. Based on the candidate routes, the shortest path can be obtained by applying a shortest path algorithm (e.g., Dijkstra's algorithm). In this study, we assumed that all the en route entry/exit points from different cruise levels that connect a common vertiport have the same two-dimensional (2-D) coordinates; they overlap each other when looking from above. The detailed steps are as follows:

1) Construct a 3-D GIS map of the region based on Light Detection and Ranging (LiDAR) data. Available airspace that is free to fly is determined by a LiDAR point cloud clustering approach, where obstacles, obstructions, and restricted airspaces are clustered into bounding boxes, in which no aircraft are allowed to enter.

2) Construct a visibility graph for any pair of en route entry and exit points on each flight level. In the visibility graph, a node represents the vertices of obstacles, and an edge represents a connection between those nodes that are not blocked by the obstacles.

3) Obtain the shortest path for each en route entry and exit point pair on each flight level. Given the visibility graph generated at each cruise level, the shortest path can be obtained by applying a shortest path algorithm.

4) Identify coordinates of spatial intersection between the shortest paths, and store the intersecting information in a database.

Figure 1 illustrates the mission profile of UAM operation and en route airways (shortest paths) at a cruise level. The vehicle takes off vertically from the vertiport, followed by the climb to the cruise level (en route) passing the en route entry point. The vehicle continues cruising until it reaches the en route exit point. Then, it descends and vertically lands at the destination vertiport. In addition to the en route conflicts (shown as red dots), this study considered potential conflicts at en route entry/exit points (shown as white circles) as well, which results in more intersection types than that described by Tang et al. [13]. Figure 2 shows three types of en route intersections based on aircraft encounters: type 1, pure intersection (intersection angle $\theta > 0$); type 2, collinear with the same direction; and type 3, collinear with opposite direction [14].

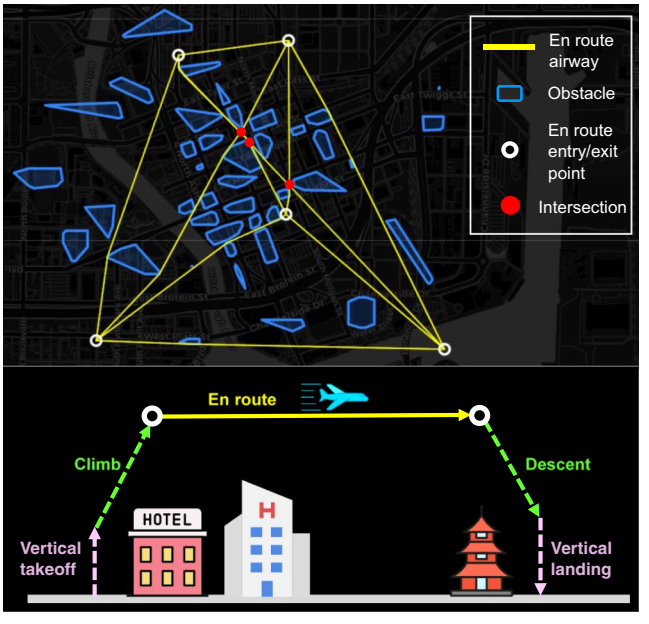

Fig. 1 Mission profile (for illustration only) and en route intersections.

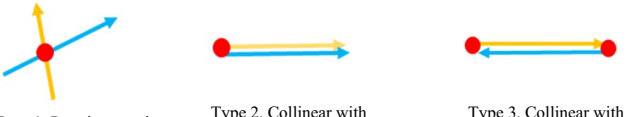

Fig. 2 En route intersection types.

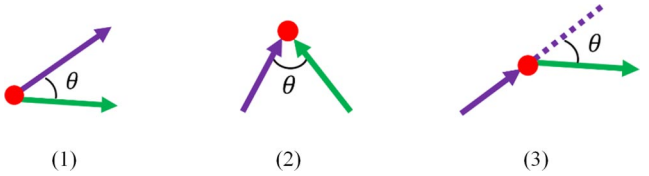

Fig. 3 Intersection types at en route entry/exit point.

When considering conflicts at en route entry/exit points, we broke them down into three cases, as shown in Fig. 3. The first two cases are two routes splitting and merging at a common en route entry/exit point, and the third is the en route entry/exit point connecting an arrival route and a departure route. All these intersection types were categorized into two groups according to the conflict detection method we used.

B. Conflict Detection

In a 2-D plane, a conflict occurs when two or more aircraft violate the minimum horizontal separation D (lateral separation D^{lateral} when intersection angle $0 < \theta < \pi$; longitudinal separation D^{long} when $\theta = 0/\pi$). We converted this spatial distance to temporal distance and detected conflicts by checking the interval between two aircraft crossing the intersecting point. For the type 1 intersection where the intersection angle is greater than zero, given aircraft speeds, intersection angle, minimum lateral separation D^{lateral}, and linearly extrapolated trajectories, the minimum temporal separation $S_{i,j}$ between aircraft at their intersecting point is computed by Vela et al. [20]:

$$S_{i,j} = \frac{D^{\text{lateral}}}{v_i v_j |\sin(\theta_{i,j})|} \sqrt{v_i^2 + v_j^2 - 2v_i v_j \cos(\theta_{i,j})} \tag{1}$$

where v_i and v_j are the aircraft speeds of aircraft i and aircraft j, respectively; $\theta_{i,j}$ is their intersection angle; and D^{lateral} is the minimum lateral separation. For intersection in Fig. 3 (3), the minimal temporal separation can also be computed by Eq. (1). For type 2 and type 3 intersections, as aircraft are flying on the same route segment, $S_{i,j}$ is computed based on the minimum longitudinal separation D^{long}, assuming two aircraft flying in the same direction on the same flight level would have the same cruise speed. Compared with type 2 and type 3 intersections, the minimum temporal separation for intersections in Fig. 3 (1) and (2) should be smaller, as two aircraft have some lateral spacing when splitting or merging at the en route entry/exit point. For simplicity, we enforce the minimum temporal separation for intersections in Fig. 3 (1) and (2) following the minimum lateral separation D^{lateral} as opposed to the larger minimum longitudinal separation D^{long}.

Let $\delta_{i,j,p}$ denote the minimum temporal separation between flights i and j at an intersecting point p. For an intersection angle greater than zero, if the interval is larger than $\delta_{i,j,p}$, then there is no conflict; for an intersection angle equal to zero (which is the type 2 intersection, collinear with the same direction), the conflict can be detected by checking the interval of two aircraft crossing either of the segment endpoints, assuming two aircraft have the same speed. Therefore, for an intersection angle greater than or equal to zero (referred to as type A), the conflict detection can be conducted the same way by checking if the interval of a pair of aircraft i, j crossing the intersecting point is greater than the minimum temporal separation $\delta_{i,j}$. The relationship is expressed in Eq. (2), where $T_{i,p}$ and $T_{j,p}$ represent the arrival times aircraft i and j reach at the intersecting point p, respectively:

$$|T_{i,p} - T_{j,p}| \geq \delta_{i,j,p} \tag{2}$$

When the intersection angle is equal to π (a type 3 intersection, collinear with opposite direction), two aircraft cannot be on the same route at the same time. The arrival times T_{i,p_1}, T_{i,p_2}, T_{j,p_1}, T_{j,p_2} of aircraft i, j passing two endpoints p_1, p_2 of the route segment are introduced for detecting conflicts. The relationships in Eq. (3) are used to detect conflict; there will be no conflicts when either of the constraints is met. Both constraints enforce that an aircraft is not on the route segment when another aircraft is on it by checking the arrival times at the two endpoints. This kind of intersection is referred to as a type B intersection.

$$T_{i,p_2} + \delta_{i,j,p_2} \leq T_{j,p_2}$$
$$\text{or}$$
$$T_{j,p_1} + \delta_{i,j,p_1} \leq T_{i,p_1} \tag{3}$$

Figure 4 summarizes the type A and type B intersections and their corresponding minimum temporal separation calculation and conflict detection method for aircraft i, j flying on the two routes given minimum lateral separation D^{lateral}, minimum longitudinal separation D^{long}, and aircraft cruise speed v. All intersections of the same type can use the same conflict detection method based on the minimum temporal separation identified from each case.

Some intersecting points might involve multiple intersection cases. In this situation, the maximum temporal separation from all different types is set as the temporal separation. For instance, Fig. 5 shows a scenario where aircraft i, j pass a vertex of an obstacle. To calculate the minimum temporal separation required for the two aircraft passing the vertex, we need to consider four cases, all of which are type A intersections in this instance. Suppose the minimum temporal separations were calculated for all four cases as δ_1, δ_2, δ_3, and δ_4, respectively. Then, the minimum temporal separation of aircraft i, j passing this intersecting point is $\max(\delta_1, \delta_2, \delta_3, \delta_4)$.

C. Flight Deconfliction

All en route intersection information is stored in a database beforehand. Given a request for a flight operation (departure vertiport, arrival vertiport, and desired departure time), the route intersection information is retrieved from the database to conduct flight deconfliction. A strategic deconfliction approach (FLA + DD) is proposed in this study to resolve

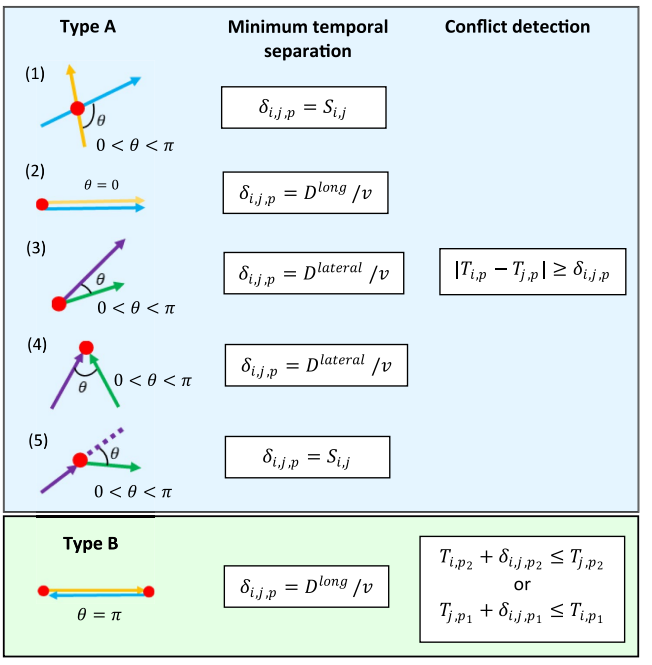

Fig. 4 Minimum temporal separation calculation and conflict detection for type A and type B intersections.

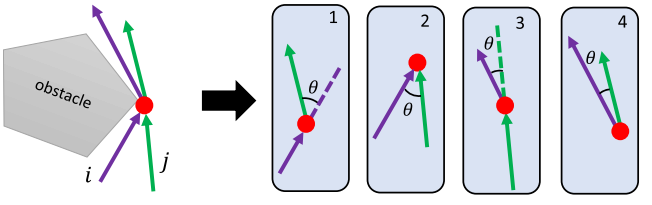

Fig. 5 Intersecting point involving multiple intersection cases.

conflicts. Consider a set of flights F operating in low-altitude urban airspace that is divided into $|H|$ flight levels. The departure time dep_i is given for each flight $i \in F$. Suppose the en route airways taken by flight i, j spatially intersect with each other at an intersecting point p, which can be either a type A or type B intersection. Let I_A, I_B denote the set of type A and type B intersections, respectively. Given the cruise speed, cruise level, departure time, and distance from the en route entry point to the intersecting point, the flying time of flight i, denoted as $t_{i,p}$, from the origin airport to the intersecting point p can be obtained. In what follows, we first describe the notation, summarizing the aforementioned set of parameters and describing the variables (Table 1). We then present the mathematical model with only FLA to deconflict flights, from which the model of FLA + DD is derived.

1. FLA Model

$$\begin{aligned}\text{Min} \sum_i \sum_h c_{i,h}^{\text{energy}} \phi_{i,h} + \sum_i \sum_h c^{\text{crew}}(t_{i,h}^{\text{flying}})\phi_{i,h} \\ + \sum_i \sum_h c^{\text{Maint.}}(t_{i,h}^{\text{flying}})\phi_{i,h}\end{aligned} \tag{4}$$

where

$$\begin{aligned}c_{i,h}^{\text{energy}} &= (P_{\text{hover}} t_{i,h}^{\text{hover}} + P_{\text{climb}} t_{i,h}^{\text{climb}} + P_{\text{cruise}} t_{i,h}^{\text{cruise}} \\ &\quad + P_{\text{descent}} t_{i,h}^{\text{descent}}) c^{\text{electricity}}; \\ t_{i,h}^{\text{flying}} &= t_{i,h}^{\text{hover}} + t_{i,h}^{\text{climb}} + t_{i,h}^{\text{cruise}} + t_{i,h}^{\text{descent}}\end{aligned}$$

subject to

$$\sum_h \phi_{i,h} = 1 \quad \forall i \in F \tag{5}$$

$$SL_{i,j,h} = (\phi_{i,h} = 1 \wedge \phi_{j,h} = 1) \quad \forall i, j \in F, \quad \forall h \in H \tag{6}$$

$$|(\text{dep}_i + t_{i,p}) - (\text{dep}_j + t_{j,p})| - \delta_{i,j,p} \geq M(SL_{i,j,h} - 1) \quad \forall p \in I_A \tag{7}$$

Table 1 Summary of notation, parameters, and variables

Sets and indices	
$\boldsymbol{i, j \in F}$	index and set of flights
$\boldsymbol{h \in H}$	index and set of flight levels
$\boldsymbol{p \in I_A}$	index and set of type A intersecting points
$\boldsymbol{p \in I_B}$	index and set of type B intersecting points
Parameters	
$\boldsymbol{c_{i,h}^{\text{energy}} \in \mathbb{R}^+}$	energy cost of flight $\boldsymbol{i}$ assigned to level $\boldsymbol{h}$
$\boldsymbol{c^{\text{electricity}}, c^{\text{crew}}, c^{\text{Maint.}} \in \mathbb{R}^+}$	electricity rate, crew hourly rate, maintenance hourly rate
$\boldsymbol{P_{\text{hover}}, P_{\text{climb}}, P_{\text{cruise}}, P_{\text{descent}} \in \mathbb{R}^+}$	power consumptions for hover, climb, cruise, and descent
$\boldsymbol{t_{i,h}^{\text{flying}} \in \mathbb{R}^+}$	flying time of flight $\boldsymbol{i}$ assigned to level $\boldsymbol{h}$
$\boldsymbol{t_{i,h}^{\text{hover}}, t_{i,h}^{\text{climb}}, t_{i,h}^{\text{cruise}}, t_{i,h}^{\text{descent}} \in \mathbb{R}^+}$	hover time, climb time, cruise time, and descent time of flight $\boldsymbol{i}$ assigned to level $\boldsymbol{h}$
$\boldsymbol{\delta_{i,j,p} \in \mathbb{R}^+}$	minimum temporal separation of flight $\boldsymbol{i, j}$ at intersecting point $\boldsymbol{p}$
$\boldsymbol{t_{i,p} \in \mathbb{R}^+}$	flying time of flight $\boldsymbol{i}$ from origin to an intersecting point $\boldsymbol{p}$
dep_i	departure time of flight $\boldsymbol{i}$
Decision variables	
$\boldsymbol{\phi_{i,h} \in \{0, 1\}}$	This variable = 1 if flight $\boldsymbol{i}$ is assigned to $\boldsymbol{h}$, and 0 otherwise.
$\boldsymbol{d_i \in \mathbb{R}_{\geq 0}}$	DD of flight $\boldsymbol{i}$
Indicator variable	
$\boldsymbol{SL_{i,j,h} \in \{0, 1\}}$	This indicator variable = 1 if flight $\boldsymbol{i}$ and flight $\boldsymbol{j}$ assigned to the same flight level $\boldsymbol{h}$, and 0 otherwise.

$$\begin{cases} u_1 \leq M_1(1 - SL_{i,j,h}) + \overline{M}_1(1 - y_1) \\ u_2 \leq M_2(1 - SL_{i,j,h}) + \overline{M}_2(1 - y_2) \\ y_1 + y_2 = 1 \\ y_1, y_2 \in \{0, 1\} \end{cases} \quad \forall p_1, p_2 \in I_B$$

$$\phi_{i,h}, SL_{i,j,h} \in \{0, 1\} \tag{8}$$

where

$$\begin{aligned} u_1 &= \text{dep}_i + t_{i,p_2} + \delta_{i,j,p_2} - \text{dep}_j - t_{j,p_2} \\ u_2 &= \text{dep}_j + t_{j,p_1} + \delta_{i,j,p_1} - \text{dep}_i - t_{i,p_1} \\ M_1 &= \max(u_1), M_2 = \max(u_2) \\ \overline{M}_1 &= \max(u_1 - M_1(1 - SL_{i,j,h})) \\ \overline{M}_2 &= \max(u_2 - M_2(1 - SL_{i,j,h})) \end{aligned}$$

The FLA model is formulated as an integer program with the objective to minimize the operating cost, which consists of energy cost, crew cost, and maintenance cost. The energy cost is the sum of hover, climb, cruise, and descent, as shown in the mission profile in Fig. 1. The decision variable $\phi_{i,h}$ determines which flight level flight f takes. Each flight is assigned to the one and only flight level expressed in constraint (5). Indicator variable $SL_{i,j,h} = 1$ if flight i and flight j take the same flight level h; otherwise $SL_{i,j,h} = 0$. Constraint (7) ensures that if flights i, j use the same level ($SL_{i,j,h} = 1$) and have a type A intersecting point ($p \in I_A$), they need to meet the minimum temporal separation $\delta_{i,j,p}$ when passing the intersecting point p. Constraint (8) ensures that if flights i, j take the same level ($SL_{i,j,h} = 1$) and have a type B intersecting point ($p \in I_B$), they are not allowed to be on the same route segment at the same time, and the minimum temporal separation must be met at either of the segment endpoints.

2. FLA + DD Model

We first introduce the DD variable $\{d_i \in \mathbb{R} | \underline{d_i} \leq d_i < \overline{d_i}\}$ for flight $i \in F$, where $\underline{d_i}$ and $\overline{d_i}$ are the lower and upper bounds of the delay. In this study, $\underline{d_i}$ is set to be zero; thus, only DD is allowed. Constraints (5) and (6) remain the same as the FLA model. We denote $t_{i,j} = \text{dep}_i + t_{i,p} - \text{dep}_j - t_{j,p}$. After introducing d_i, constraint (7) in the FLA model becomes

$$|t_{i,j} + d_i - d_j| \geq \delta_{i,j,p} + M(SL_{i,j,h} - 1) \quad \forall p \in I_A$$

The preceding constraint is nonlinear and can be linearized as follows:

$$\begin{cases} (t_{i,j} + d_i - d_j) + \overline{M_1} y \geq \delta_{i,j,p} + M(SL_{i,j,h} - 1) \\ -(t_{i,j} + d_i - d_j) + \overline{M_2}(1 - y_1) \geq \delta_{i,j,p} + M(SL_{i,j,h} - 1) \\ y_1 \in \{0, 1\} \end{cases} \quad \forall p \in I_A$$

where

$$\begin{aligned} t_{i,j} &= \text{dep}_i + t_{i,p} - \text{dep}_j - t_{j,p} \\ M &= \max(\delta_{i,j,p} - |t_{i,j} + d_i - d_j|) \\ \overline{M_1} &= \max(-t_{i,j} - d_i + d_j + \delta_{i,j,p}) \\ \overline{M_2} &= \max(t_{i,j} + d_i - d_j + \delta_{i,j,p}) \end{aligned}$$

Constraint (8) in the FLA model after introducing d_i becomes

$$\begin{cases} u_1 + d_i - d_j \leq M_3(1 - SL_{i,j,h}) + \overline{M}_3(1 - y_2) \\ u_2 + d_j - d_i \leq M_4(1 - SL_{i,j,h}) + \overline{M}_4 y_2 \\ y_2 \in \{0, 1\} \end{cases} \quad \forall p_1, p_2 \in I_B$$

where

$$M_3 = \max(u_1 + d_i - d_j)$$
$$M_4 = \max(u_2 + d_j - d_i)$$
$$\overline{M}_3 = M_3$$
$$\overline{M}_4 = M_4$$

In summary, the formulation of the FLA + DD model has the same objective function as the FLA model, and the constraints are as follows:

subject to

$$\sum_h \phi_{i,h} = 1 \quad \forall i \in F \tag{9}$$

$$SL_{i,j,h} = (\phi_{i,h} = 1 \wedge \phi_{j,h} = 1) \quad \forall i, j \in F, \quad \forall h \in H \tag{10}$$

$$\begin{cases} (t_{i,j} + d_i - d_j) + \overline{M}_1 y_1 \geq \delta_{i,j,p} + M(SL_{i,j,h} - 1) \\ -(t_{i,j} + d_i - d_j) + \overline{M_2}(1 - y_1) \geq \delta_{i,j,p} + M(SL_{i,j,h} - 1) \quad \forall p \in I_A \\ y_1 \in \{0, 1\} \end{cases} \tag{11}$$

where

$$t_{i,j} = \text{dep}_i + t_{i,p} - \text{dep}_j - t_{j,p}$$
$$M = \max(\delta_{i,j,p} - |t_{i,j} + d_i - d_j|)$$
$$\overline{M_1} = \max(-t_{i,j} - d_i + d_j + \delta_{i,j,p})$$
$$\overline{M_2} = \max(t_{i,j} + d_i - d_j + \delta_{i,j,p})$$

$$\begin{cases} u_1 + d_i - d_j \leq M_3(1 - SL_{i,j,h}) + \overline{M}_3(1 - y_2) \\ u_2 + d_j - d_i \leq M_4(1 - SL_{i,j,h}) + \overline{M}_4 y_2 \\ y_2 \in \{0, 1\} \\ \underline{d_i} \leq d_i \leq \overline{d_i} \end{cases} \quad \forall p_1, p_2 \in I_B \tag{12}$$

where

$$u_1 = \text{dep}_i + t_{i,p_2} + s_{i,j,p_1} - \text{dep}_j - t_{j,p_2}$$
$$u_2 = \text{dep}_j + t_{j,p_1} + s_{i,j,p_1} - \text{dep}_i - t_{i,p_1}$$
$$M_3 = \max(u_1 + d_i - d_j)$$
$$M_4 = \max(u_2 + d_j - d_i)$$
$$\overline{M}_3 = M_3$$
$$\overline{M}_4 = M_4$$

It should be noted that the DD is not included in the flying time, as it is assumed that the crew and maintenance will be notified by the PSU in advance of the delay. Thus, no additional flying hours will be expended by them.

3. *Rolling-Window Algorithm*

A rolling-window algorithm is developed to break down the problem into a number of smaller problems. The time period is divided into a number of time windows $T: (t_1, t_2, \ldots, t_n)$, and the conflicts are solved sequentially at each time window for flights departing in that window and for flights departing beforehand but not landing yet.

The algorithm begins by planning the fights scheduled to depart within the first time window. To do so, it solves the FLA + DD model by calling a commercial solver, which assigns each flight a level and calculates DDs. For flights that are not scheduled to land during the first time window, the algorithm will impose additional constraints to the FLA + DD model in the next time window to ensure that the solutions obtained in the current window (i.e., FLA and DD) are carried forward. Moving on to the second time window, the algorithm runs the FLA + DD model to find solutions for flights scheduled for that window as well as flights that are still in the air from prior time windows. The solutions for flights from previous windows remain the same, as additional constraints are added to maintain their previously obtained solutions. This iterative process continues until all flights have landed by the end of the final time window.

Algorithm 1: Rolling window algorithm

input: Type A, Type B intersection: I_A, I_B
Time windows: $t \in T$
Flights: $i \in F$
Flights scheduled to depart in time window $t: F[t]$
Flight levels: $h \in H$
output: flight i assigned to level $h: \phi_{i,h} \in \Phi$
flight i departure delay: $d_i \in D$
flight i and j take same flight level: $SL_{i,j} \in SL$
initialization:

$t \leftarrow 0$
$F_0^* \leftarrow \varnothing$ # flights not landing in the current time window
$\Phi_0^* \leftarrow \varnothing$ # level assignment of flights not landing in the current time window
$D_0^* \leftarrow \varnothing$ # departure delay of flights not landing in the current time window
while $t \leq |T|$ **do**
  $F_t \leftarrow F_{t-1}^* \cup F[t]$
  $\Phi_t \leftarrow \Phi_{t-1}^* \cup \Phi[t]$
  $D_t \leftarrow F_t$
  # indicator variable set among $F[t]$ by the Cartesian product
  $SL_{t,t} \leftarrow F[t] \times F[t] \times H$
  # indicator variable set between $F[t]$ and F_{t-1}^* by Cartesian product for
  for i, h in Φ_{t-1}^* **do**
    conduct Cartesian product between $F[t]$, i, and h.
    append results to $SL_{t,t-1}$
  $SL_t \leftarrow SL_{t,t} \cup SL_{t,t-1}$
  # Create conflict set for Type A and Type B in the current time window
  C_typeA $\leftarrow \varnothing$
  C_typeB $\leftarrow \varnothing$
  for i, j, h in SL_t **do**
    if *flight i, j not temporally overlapping with each other* **do**
      $\text{OD}(i) \leftarrow$ retrieve OD name of flight i
      $\text{OD}(j) \leftarrow$ retrieve OD name of flight j
      if $(\text{OD}(i), \text{OD}(j), h)$ *in* I_A **then**
        append (i, j, h) to C_typeA and SL_t^c
      else if $(\text{OD}(i), \text{OD}(j), h)$ *in* I_B **then**
        append (i, j, h) to C_typeB and SL_t^c
  $y \leftarrow C$_typeA
  $y1, y2 \leftarrow C$_typeB
  build the flight level assignment + departure delay model
    add additional constraints to enforce flights in F_{t-1}^* taking their assigned level from $t-1$
    add additional constraints to enforce flights in F_{t-1}^* delay same as from $t-1$
    solve the problem by a commercial solver
    return Φ_t, D_t
  for i, h in Φ_t **do**
    if $\Phi_t(i, h) > 0.5$ and *mission not completed in* $t+1$ **then**
      append (i, h) to Φ_t^*
  for i, h in Φ_t^* **do**
    append (i) to F_t^*
  for i in F_t^* **do**
    append (i) to D_t^*

D. Electric Vertical Takeoff and Landing Power Requirement

To obtain the energy cost for each flight, the power requirement for each flight segment needs to be known. The power requirements for hover and cruise are calculated from Eqs. (13) and (14), respectively, according to aircraft specifications [21]. The hover power is determined from takeoff mass W, correction factor for interference from the fuselage f, figure of merit (FM), disk loading δ, air density ρ, and hover system efficiency η_h. (We assume the takeoff segment requires the same power as hover.) The cruise power is determined by takeoff mass W, cruise velocity V, cruise system efficiency η_c, and lift-to-drag ratio (L/D). Climb and descent require 140 and 20% of cruise power, respectively [22,23]. The hover system efficiency η_h used in this study is a metric that takes into account both power-train efficiency and propulsive efficiency, and FM is the ratio of ideal induced power to actual power in hover [24,25]. It is worth noting that multirotor aircraft consume more energy during descent compared to winged electric vertical takeoff and landing (EVTOL) vehicles, exceeding 20% of their cruise power. However, we acknowledge that due to the limited available data, our assumption is that both multirotor and winged EVTOL vehicles require 20% of their cruise power during descent. Further research and data gathering may allow for a more accurate estimation of the power requirements for these types of aircraft during descent:

$$P_{\text{hover}} = \left(\frac{fW}{FM}\sqrt{\frac{f\delta}{2\rho}}\right)/\eta_h \tag{13}$$

where W is the takeoff mass, f is the correction factor for interference from the fuselage, FM is the figure of merit, δ is the disk loading, ρ is the air density, and η_h is the hover system efficiency.

$$P_{\text{cruise}} = \frac{WV}{\frac{L}{D}\eta_c} \tag{14}$$

where V is the cruise velocity, and η_c is the cruise system efficiency.

III. Experimental Setup

We demonstrate the predeparture flight planning on our proposed airspace structure for medium- to high-density UAM operations. In the experiment, four available cruise levels (CL1, CL2, CL3, and CL4) were constructed starting from 500 ft with 50, 40, 30, and 20 randomly generated obstacles from the bottom level to the top (shown in Fig. 6). Flights were set to randomly depart from an origin to a destination vertiport in a 30 min window. The FLA + DD model was solved using both the Gurobi solver and the rolling-window algorithm under different operation densities (represented by number of flights to plan and number of vertiports). We also solved the FLA model using the Gurobi solver to compare the computation times of the different models. When the DD is set to zero, solving the FLA + DD model is essentially the same as solving the FLA model.

Experiments were conducted for three fleets of EVTOL vehicles: Joby (tilt-rotor), NASA quadrotor concept (multirotor), and Lilium (tilt duct). All accommodated a similar number of occupants (Joby, five seats; NASA quadrotor, six seats; and Lilium, seven seats). Equations (14) and (15) were used to calculate the power requirement for hover and cruise based on aircraft specifications found from the EVTOL manufacturers and existing literature (see Table 2). We estimated the disk loading of Joby at 9.5 psf based on its advertised gross weight and propeller diameter. It was assumed that all three aircraft have the same correction factor for interference from the fuselage and FM [21,24]. The hover system efficiency and cruise system efficiency of Joby and NASA quadrotor were assumed to be 0.63 and 0.765, respectively [25]. Although Joby's L/D was unknown, we investigated other similar EVTOL vehicles to speculate a range. The conceptual lift + cruise aircraft designed by NASA has an L/D of 7.9 [26]. It is believed that a tilt-rotor with many propellers will not be as efficient in cruise as a lift + cruise configuration, which has a fixed wing. Nevertheless, Archer's tilt-rotor EVTOL, a configuration similar to Joby, has a design L/D of 12. In optimistic speculation, we set Joby's L/D between 7.9 and 12 in this study. In the experiment, the power requirement was calculated for three different L/D values (12, 10, and 7.9) for Joby. Table 3 shows the computed power requirement by flight segment for Joby, NASA quadrotor, and Lilium using sea-level standard atmosphere.

Given the cost and operational parameters in Table 4 and flight times in each flight segment, the operating cost (including energy, crew, and maintenance) was obtained for each flight of a specific EVTOL type [22,24,27]. Although a pilot is anticipated to be onboard in the early stage of UAM operations, pilotless operations are envisioned for the mature stage of UAM operations. Therefore, the minimum crew rate was derived from the mature stage, where only ground crew cost was

Table 2 Aircraft specification and parameters for power requirement calculation

Specification/parameters	Joby	NASA quadrotor [24,26]	Lilium [23]
Configuration	Tilt-rotor	Multirotor	Tilt duct
Seats	5	6	7
Maximum takeoff mass W, lb	4800	7221	7000
Disk loading δ, psf	9.5	3	243.53
Correction factor f [21]	1.03	1.03	1.03
FM [24]	0.7	0.7	0.7
Hover system efficiency	0.63	0.63 [25]	0.59
Cruise speed V, kt	174	91	152
L/D	7.9–12	5.8	18.26
Cruise system efficiency	0.765	0.765 [25]	0.65

Table 3 Power requirements at different flight segments

	Joby			NASA quadrotor	Lilium [23]
L/D	12	10	7.9	5.8	18.26
Hover power, kW	690	690	690	583	2570
Cruise power, kW	208	250	316	339	224
Climb power, kW	291	350	442	475	511
Descent power, kW	42	50	63	68	53

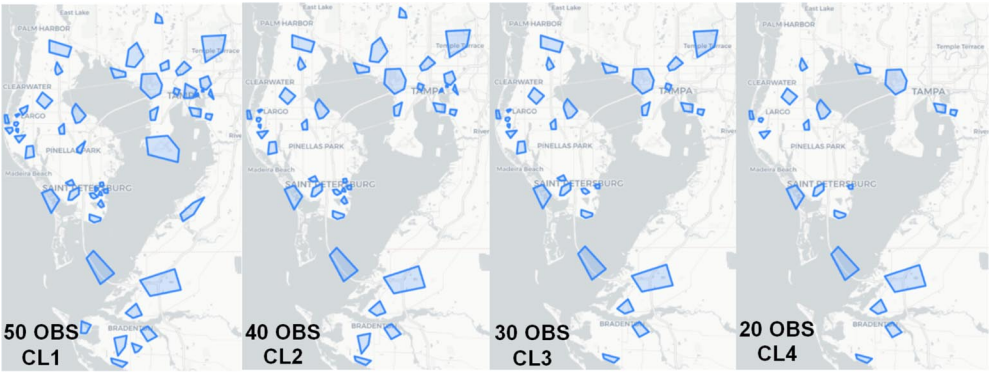

Fig. 6 Randomly generated obstacles for four cruise levels in Tampa Bay, Florida area.

Table 4 Cost and operational parameters

Parameter	Minimum value	Base-case value	Maximum value	Source
Electricity cost	\$0.1/kWh	\$0.2/kWh	\$0.3/kWh	[22]
Flight hours	\$1,500/yr	\$1,500/yr	\$1,500/yr	[22]
Pilot salary	\$0/yr	\$35,000/yr	\$70,000/yr	
Ground crew salary	\$25,000/yr	\$25,000/yr	\$25,000/yr	
Crew cost	\$17/flight hour	\$40/flight hour	\$63/flight hour	
Mechanic wrap rate	\$60	— —	\$100	[22]
Maintenance man-hour/flight hour	0.25	— —	1	
Maintenance cost	\$15/h	\$57.5/h	\$100/h	
Vertical takeoff	— —	ROC 100 ft/min for 30 s	— —	[24]
Vertical landing	— —	ROD 100 ft/min for 30 s	— —	
Climb	— —	ROC 1,000 ft/min	— —	[27]
Descent	— —	ROD 1,000 ft/min	— —	

taken into account; the maximum crew rate was derived from the early stage, where both pilot and crew costs were taken into account. We assumed constant flight hours and ground crew salary in computing the crew hourly rate. The mission profile started with a 30 s vertical takeoff at a rate of climb (ROC) of 100 ft/m before an ROC of 1000 ft/m to cruise level. After cruise flight, the aircraft descended at a rate of descent (ROD) of 1000 ft/m until a final 100 ft/m ROD vertical landing of 30 s. We conducted further analysis to investigate the sensitivity of operating cost to three key cost parameters (electricity price, crew hourly rate, and maintenance hourly rate).

The relationships of departure delay bound (maximum departure delay allowed) vs operating cost saving and departure delay bound vs delay cost to passengers are examined, as is the tradeoff between operating cost saving and passenger delay cost.

IV. Results

A. Computation Times

The FLA model was solved by Gurobi 9.1.2, and the FLA + DD model was solved by Gurobi and by the rolling-window algorithm on a PC with Intel® Core™ i7-10700 CPU 2.90 GHz 16 GB RAM. Different Virtual Processor (VP) configurations were used to examine the sensitivity of run time to computing architecture. The results from Table 5 were obtained from the base case with a flight-level vertical separation of 100 ft and a DD bound of 5 min with no departures ahead of the scheduled departure time allowed.

The FLA model took very little time to deconflict the flights when operation density was low (i.e., scenarios with small numbers of flights and large numbers of vertiports). However, for the scenario of 500 flights and 10 vertiports, some conflicts could not be resolved simply by assigning flights to different flight levels.

For the FLA + DD model, the Gurobi solver took a much longer time to solve the problem, particularly when the number of flights was greater than 400 and the number of vertiports was less than 20. However, with more vertiports (30 vertiports), the computation time, about 1 min, was acceptable for a larger number of flights. Compared to the Gurobi solver, the rolling-window algorithm largely reduced the computation time for high-density operations, in which the number of flights was large and the number of vertiports was small. It should be noted that the rolling-window algorithm divided the whole planning phase into several time windows, and the conflicts were solved sequentially at each time window by the FLA + DD model. The MILP problem was solved by the Gurobi solver to optimality in each time window.

B. Sensitivity Analysis

Three key cost parameters (electricity price, crew hourly rate, and maintenance hourly rate) were individually varied over a bounded range. The base case used the medians of these parameters. The low input and high input took the lower bound and upper bound, respectively. Electricity price ranged from \$0.1 to \$0.3/kWh, the crew hourly rate ranged from \$16.67 to \$63.33/h, and the maintenance hourly rate ranged from \$15 to \$100/h. The sensitivity analysis was conducted based on outcomes from the FLA + DD model, which was solved by the rolling-window algorithm for planning 500 flights in a 30 min window.

A higher L/D reduces the energy cost because of the more efficient cruise flight, which contributes to a decrease in operating cost (see Appendix, Fig. A1). Figure 7 shows the operating cost comparison between Lilium, NASA quadrotor, and Joby's most energy-optimistic case (with the L/D of 12). As the cost parameter increased from low to high, approximately a linear growth of the operating cost was observed because of the linear relationship between the operating cost and the cost parameters. However, the solutions (FLA and DD) reacting to the increase/decrease in cost parameters resulted in nonlinearity in operating cost change. A larger variation in cost parameters tends to have a bigger impact on operating cost (e.g., maintenance cost). In the base case, maintenance cost had the largest share of the operating cost for Joby, and energy cost had the largest share for Lilium and NASA quadrotor (see Fig. 8). For Joby, the maintenance cost share increased to 52.2% of the operating cost with a high maintenance rate (\$100/h) but decreased to 14.1% with a low maintenance rate (\$15/h). For Lilium and NASA quadrotor, the energy cost share increased to 62.9 and 56.1% of the operating cost, respectively, with a low maintenance rate, but decreased to 32.3 and 26.5%, respectively, with a low electricity price (\$0.1/kWh).

Although lower cruise levels tend to lead to longer horizontal cruise distances, as the EVTOL vehicles need to avoid more obstructions, the longer climb and descent time for higher altitudes could offset the additional horizontal distance to some extent, making the mission time distributions almost identical to each other for different cruise levels (see Fig. 9). This makes the DD a relatively small effect on the operating cost, as delaying the departure time may gain the aircraft an opportunity to fly at the optimal flight level rather than fly at a higher flight level to resolve a conflict. However, the small

Table 5 Computation times (s) of different operation densities for 30 min planning windows

	FLA			FLA + DD					
	Gurobi solver			Gurobi solver			Rolling-window algorithm		
Number of flights	10 VPs	20 VPs	30 VPs	10 VPs	20 VPs	30 VPs	10 VPs	20 VPs	30 VPs
100	0.02	0.02	0.02	0.08	0.09	0.06	0.8	0.6	0.6
200	0.11	0.05	0.03	7.9	0.4	0.45	3.3	2.3	2.1
300	2.4	0.12	0.08	317	2	3.02	7.7	6.9	4.8
400	281.2	0.75	0.2	>1000	116.1	18.8	15.4	9.2	8.4
500	Infeasible	47.3	4.2	>1300	>500	59.2	34.4	14.8	13.3

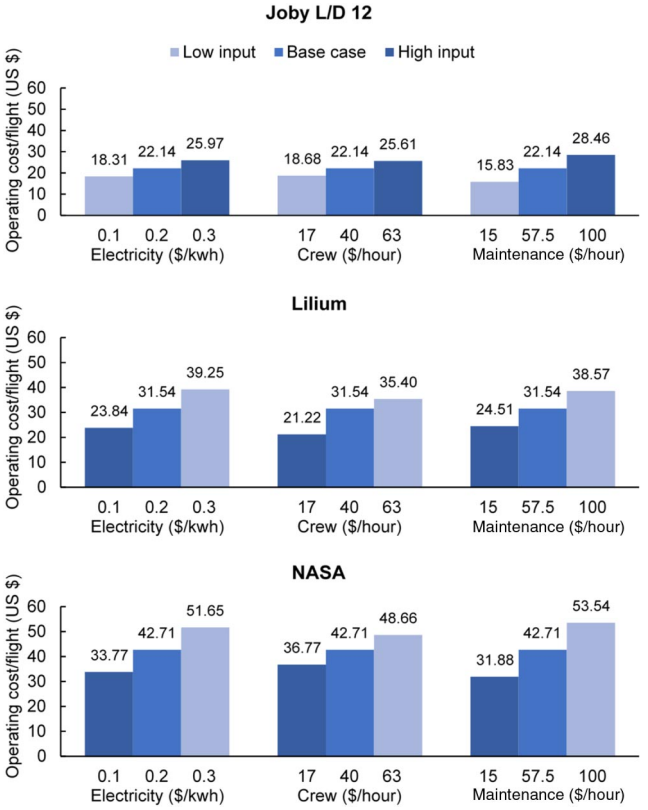

Fig. 7 Sensitivity analysis for operating cost per flight (vertical separation 100 ft; DD bound 5 min).

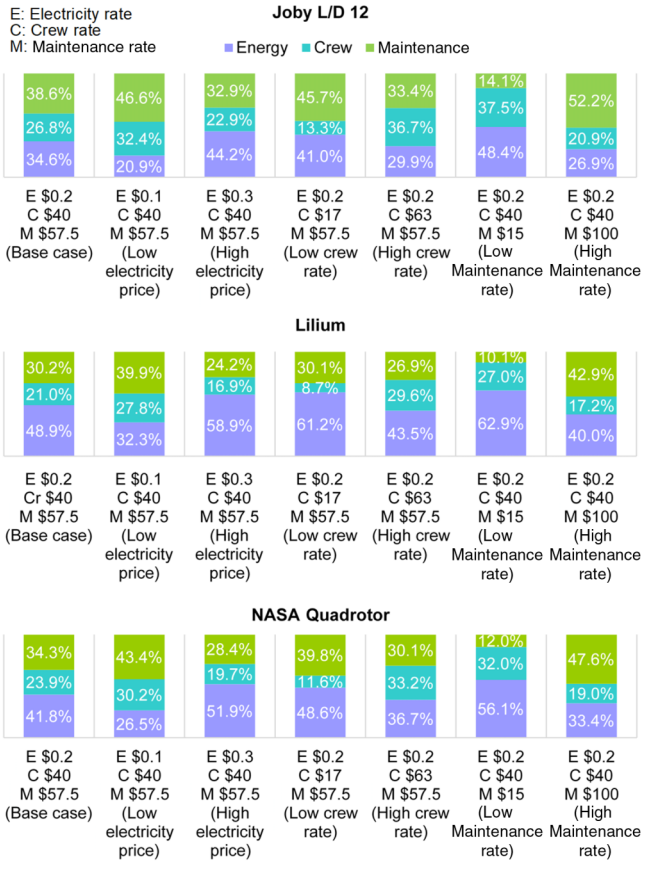

Fig. 8 Operating cost breakdown (vertical separation 100 ft; DD bound 5 min).

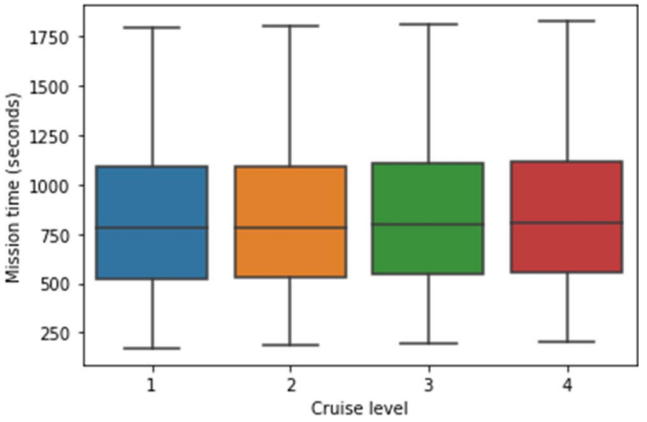

Fig. 9 Mission times at different cruise levels for 500 flights.

mission time differences for different flight levels weaken the benefits gained from DD. A larger DD bound is expected to save more operating cost (although very small from the base case with a vertical separation of 100 ft) but at the price of increasing delay cost to passengers. Thus, we explored the tradeoff between operating cost saving and delay cost to passengers with varying vertical separations and DD bounds (maximum DD allowed). According to the recommended value of travel time savings ($20.30–$30.50 for local business travel by surface modes) from the U.S. Department of Transportation [28], considering other personal travel might also use this service, the lower bound of $20.30 was used to estimate the DD cost to passengers, as business travelers are anticipated to be the biggest users of UAM services. The DD cost was computed for different passenger load factors (PLFs) as 0.5, 0.65, and 0.8.

We first analyzed the relationship between operating cost savings and DD bounds (see Fig. 10). The operating cost savings with 300 ft vertical separation were larger than those with 100 ft vertical separation, as can be seen in the figure. With a 3 min DD bound, the DD saved nearly $0.50 per flight with 300 ft separation for Lilium and only about $0.15 per flight with 100 ft separation. Lilium and NASA quadrotor had the highest and lowest operating savings from DD at both 100 and 300 ft flight-level spacing, respectively. For Joby with different cruise flight efficiency, less operating cost saving was obtained when its cruise flight required less power (higher L/D). The operating cost saving saw a quick growth as the DD bound extended to 30 s or 1 min, depending on the vertical spacing. After that, the growth slowed down and almost leveled out. Compared to the operating cost, although the operating cost savings from DDs seem small, the primary benefit of DDs is to the additional flexibility they provide to resolve conflicts, which cannot be directly quantified in terms of operating costs. While variations in DDs may not result in significant differences in operating costs, the cost of delays to passengers can vary significantly. Therefore, it is essential to explore the relationship between delay bound and passenger costs.

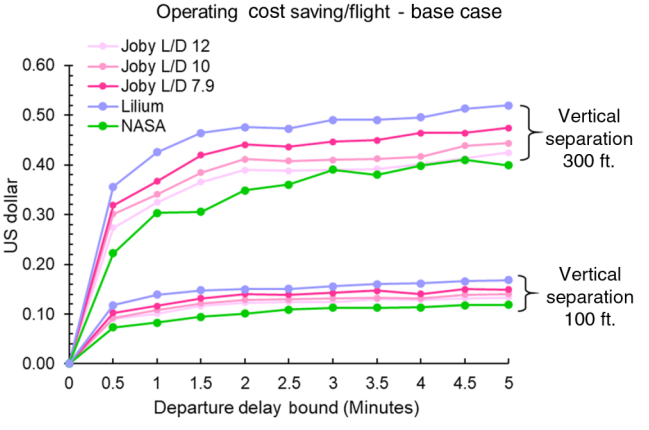

Fig. 10 Operating cost saving per flight given different DD bounds.

Next, we analyzed the relationship between delay cost to passengers and DD bound and compared the operating cost saving and delay cost to investigate the tradeoff between them. Figure 11 shows the base case for three EVTOL vehicles with 100 and 300 ft flight-level spacing. The high and low inputs of maintenance rate defined the upper and lower bounds of the operating cost savings among the cost parameters (electricity price, crew hourly rate, and maintenance hourly rate). For the base cases of the three EVTOL vehicles, the operating cost saving trend line crosses the delay cost trend line at some point. Before this crossing, more operating savings were gained than the cost of delay to passengers. For airspace structure with 300 ft vertical spacing, more benefits can be gained by waiting on the ground than with 100 ft vertical spacing (see Fig. 10). Beyond the DD bound of 1 min, we saw a swift increase in delay cost as the DD bound increased, while the operating cost saving saw a very difficult growth that almost leveled out. This suggests that care should be taken when determining the DD bound because the operating cost saving might nearly stop growing (or barely grow) after imposing a small increase in delay bound. Although more operating savings can be obtained with a larger DD bound, a slight increase in DD bound could result in a big jump in passenger delay cost but only marginal operating cost saving.

We estimated the crossover points of the operating cost saving and DD cost trend lines for the base case, high input of maintenance rate ($100/h), and low input of maintenance rate ($15/h), where the high and low maintenance rates created the trend lines of maximal and minimal operating cost savings, respectively. Figure 12 shows there is only one

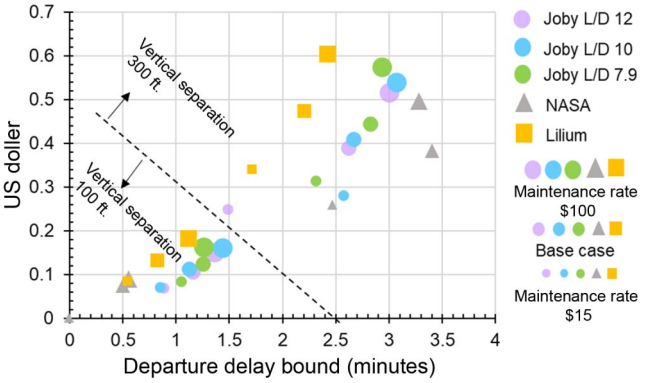

Fig. 12 Crossover points of operating cost saving and DD cost trend lines (PLF: 0.5).

crossover point at the origin of coordinates, indicating that the operating cost saving trend line met the DD cost trend line when allowing DD (DD bound greater than 0) for all cases, except for the case of NASA quadrotor with a low maintenance rate and a vertical separation of 100 ft. It can be seen that the crossover point emerged at a higher DD bound with more operating cost saving when the maintenance rate increased. This implies that we can set the DD bound to a higher value to obtain more operating cost saving that offsets the delay cost increase as the operating cost per flight rises. The crossover point can serve as a reference for decision-makers in determining the DD bound.

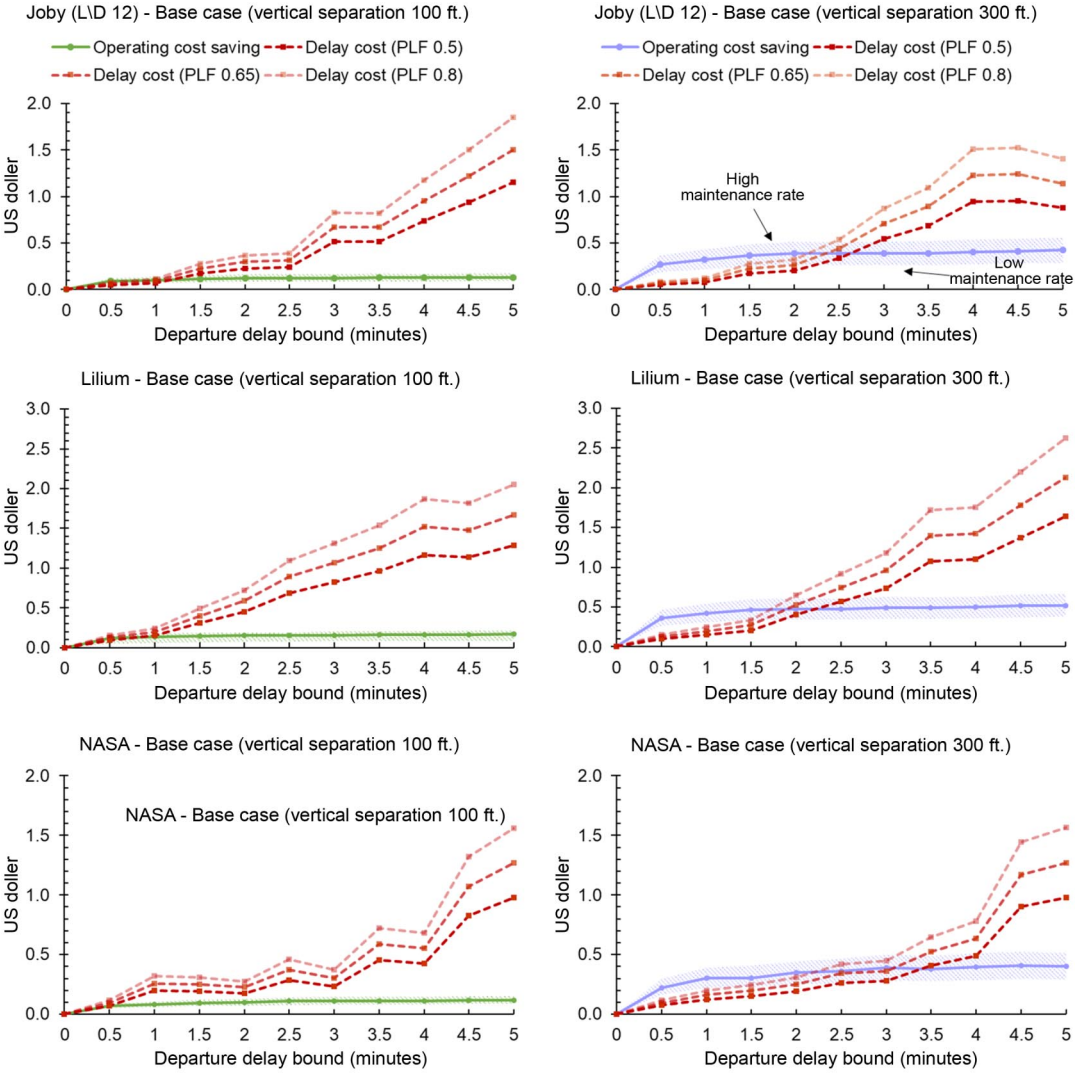

Fig. 11 Tradeoff between operating cost savings and passenger delay costs.

V. Conclusions

To be able to provide predeparture planning services for medium- to high-density UAM operations (UML of 4 and above), this study proposed airspace model and strategic deconfliction approaches for generating predeparture conflict-free four-dimensional flight trajectories, which can be further developed into an automated flight planning tool for PSU. A semistructured scalable airspace design (i.e., a layered airspace topology) was first proposed, with direct routes between vertiports, avoiding only physical obstacles, such as buildings, obstructions, and restricted airspace using the visibility graph method. When constructing the airspace network, not only the conflicting points between different en route airways were considered but also the conflicts at the en route entry/exit points, which greatly increases the number of potential conflicts that need to be taken into account. Using the proposed airspace network, strategic deconfliction approaches, fight level assignment, and DD were applied to ensure predeparture conflict-free flight. A mixed-integer programming model was proposed with the objective of minimizing the operating cost of UAM operations, aiming at the common interest of PSU and UAM operators. A rolling-window algorithm was developed to solve this deconfliction problem.

Experiments were conducted to demonstrate the predeparture flight planning for medium- to high-density UAM operations. From the sensitivity analysis, an approximate linear growth of operating cost has been seen, as the cost parameter increased from low to high. The solutions (FLA and DD) that reacted to the increase/decrease in cost parameters contribute to the nonlinearity of the operating cost change. By analyzing the relationship between passenger delay cost and DD bound and the tradeoff between operating cost saving and DD bound, it has been found that while operating savings can be gained with an increased DD bound, this could result in a big increase in passenger delay cost. The crossover point of the two trend lines of operating cost saving and DD cost can serve as a reference for decision-makers in determining the DD bound. The sensitivity analysis can provide a valuable tool for stakeholders when making operational decisions.

In future research, in addition to energy cost, crew cost, and maintenance cost, operating cost may include costs related to battery reserve. The deconfliction model developed in this study is a deterministic model, assuming that the aircraft can follow the assigned route at a predefined speed and reach any location at a certain time without considering uncertainties. Flight planning needs to take the uncertainties caused by, for instance, weather into account. In this study, three different PLFs were assumed. In fact, for on-demand operations, PLF is correlated with the waiting times on the ground. A larger wait time or DD tends to load more passengers in the aircraft, on average, which will generate more revenue per flight. When determining the DD bound, in addition to operating cost, other factors, such as revenue, should also be taken into consideration.

Appendix: Joby Sensitivity Analysis

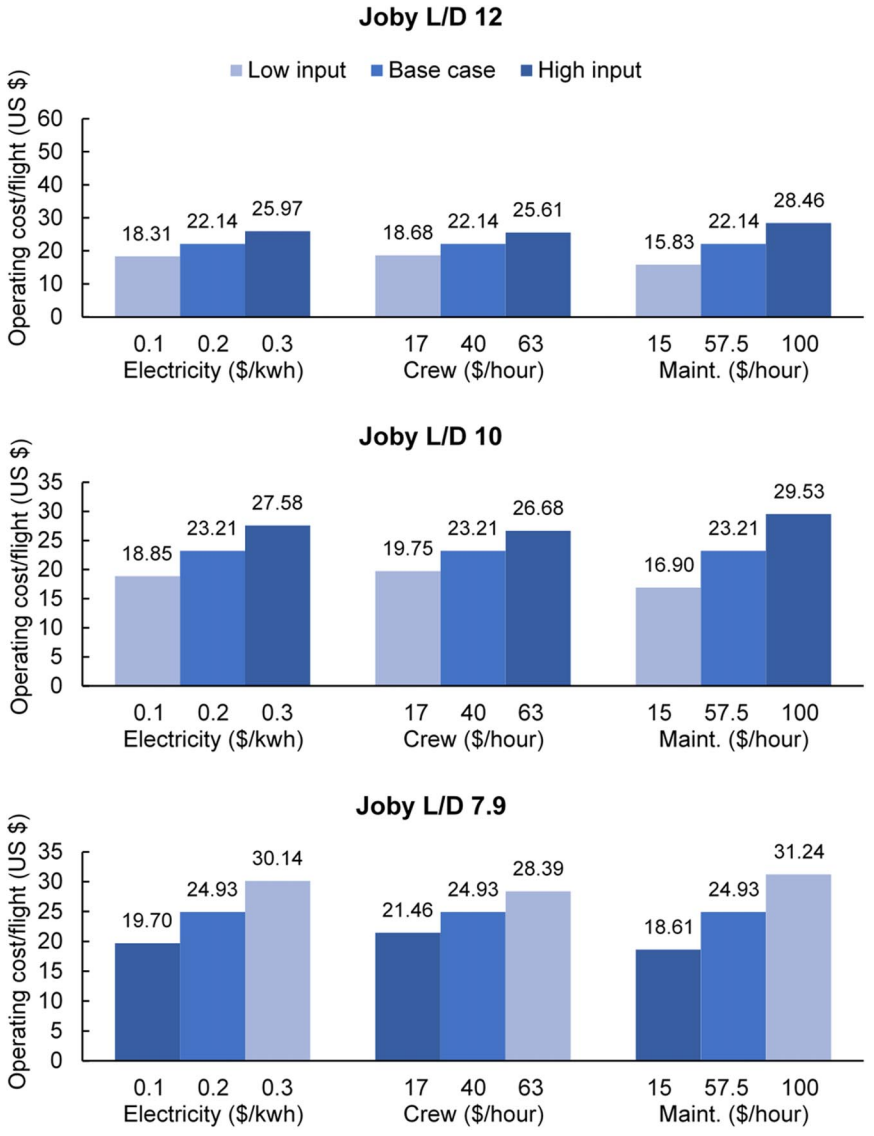

Fig. A1 Sensitivity analysis for operating cost with different L/D for Joby.

References

[1] Goodrich, K. H., and Theodore, C. R., "Description of the NASA Urban Air Mobility Maturity Level (UML) Scale," *AIAA SciTech 2021 Forum*, AIAA Paper 2021-1627, Jan. 2021. https://doi.org/10.2514/6.2021-1627

[2] Hunter, G., and Wei, P., "Service-Oriented Separation Assurance for Small UAS Traffic Management," *Integrated Communications, Navigation and Surveillance Conference (ICNS)*, IEEE, New York, 2019, pp. 1–11. https://doi.org/10.1109/ICNSURV.2019.8735165

[3] Andrews, J. W., Welch, J. D., and Erzberger, H., "Safety Analysis for Advanced Separation Concepts," *Air Traffic Control Quarterly*, Vol. 14, No. 1, 2006, pp. 5–24. https://doi.org/10.2514/atcq.14.1.5

[4] Jardin, M. R., "Analytical Relationships Between Conflict Counts and Air-Traffic Density," *Journal of Guidance, Control, and Dynamics*, Vol. 28, No. 6, 2005, pp. 1150–1156. https://doi.org/10.2514/1.12758

[5] Hoekstra, J. M., van Gent, R. N., and Ruigrok, R. C., "Designing for Safety: The 'Free Flight' Air Traffic Management Concept," *Reliability Engineering & System Safety*, Vol. 75, No. 2, 2002, pp. 215–232. https://doi.org/10.1016/S0951-8320(01)00096-5

[6] Sacharny, D., and Henderson, T. C., "A Lane-Based Approach for Large-Scale Strategic Conflict Management for UAS Service Suppliers," *2019 International Conference on Unmanned Aircraft Systems (ICUAS)*, IEEE, New York, June 2019, pp. 937–945.

[7] Jang, D.-S., Ippolito, C. A., Sankararaman, S., and Stepanyan, V., "Concepts of Airspace Structures and System Analysis for UAS Traffic Flows for Urban Areas," *AIAA Information Systems—AIAA Infotech@ Aerospace*, AIAA Paper 2017-0449, Jan. 2017. https://doi.org/10.2514/6.2017-0449

[8] Anon., "UAM Concept of Operations v1.0," 2020, https://nari.arc.nasa.gov/sites/default/files/attachments/UAM_ConOps_v1.0.pdf [retrieved 15 Jan. 2022].

[9] Bertram, J., Wei, P., and Zambreno, J., "Scalable FastMDP for Pre-Departure Airspace Reservation and Strategic De-Conflict," *AIAA SciTech 2021 Forum*, AIAA Paper 2021-0779, Jan. 2021. https://doi.org/10.2514/6.2021-0779

[10] Geister, D., and Korn, B., "Density Based Management Concept for Urban Air Traffic," *2018 IEEE/AIAA 37th Digital Avionics Systems Conference (DASC)*, IEEE, New York, 2018, pp. 1–9. https://doi.org/10.1109/DASC.2018.8569491

[11] Li, A., and Hansen, M., "Obstacle Clustering and Path Optimization for Drone Routing," *9th International Conference for Research in Air Transportation*, FAA/EUROCONTROL, 2020, pp. 1–8.

[12] Dai, W., Pang, B., and Low, K. H., "Conflict-Free Four-Dimensional Path Planning for Urban Air Mobility Considering Airspace Occupancy," *Aerospace Science and Technology*, Vol. 119, Dec. 2021, Paper 107154. https://doi.org/10.1016/j.ast.2021.107154

[13] Tang, H., Zhang, Y., Mohmoodian, V., and Charkhgard, H., "Automated Flight Planning of High-Density Urban Air Mobility," *Transportation Research Part C: Emerging Technologies*, Vol. 131, Oct. 2021, Paper 103324. https://doi.org/10.1016/j.trc.2021.103324

[14] Sunil, E., Hoekstra, J., Ellerbroek, J., Bussink, F., Nieuwenhuisen, D., Vidosavljevic, A., and Kern, S., "Metropolis: Relating Airspace Structure and Capacity for Extreme Traffic Densities," *Proceedings of the 11th USA/Europe Air Traffic Management Research and Development Seminar (ATM2015)*, FAA/EUROCONTROL, June 2015, https://hal-enac.archives-ouvertes.fr/hal-01168662 [retrieved 9 May 2023].

[15] Anon., "Supporting Safe and Secure Drone Operations in Europe: A Preliminary Summary of SESAR U-Space Research and Innovation Results (2017–2019)," Publication Office, 2020, https://data.europa.eu/doi/10.2829/695079 [retrieved May 2022].

[16] Zhu, G., and Wei, P., "Pre-Departure Planning for Urban Air Mobility Flights with Dynamic Airspace Reservation," *AIAA Aviation 2019 Forum*, AIAA Paper 2019-3519, June 2019. https://doi.org/10.2514/6.2019-3519

[17] Bertram, J., and Wei, P., "Distributed Computational Guidance for High-Density Urban Air Mobility with Cooperative and Non-Cooperative Collision Avoidance," *AIAA SciTech 2020 Forum*, AIAA Paper 2020-1371, Jan. 2020.

[18] Yang, X., and Wei, P., "Scalable Multi-Agent Computational Guidance with Separation Assurance for Autonomous Urban Air Mobility," *Journal of Guidance, Control, and Dynamics*, Vol. 43, No. 8, 2020, pp. 1473–1486. https://doi.org/10.2514/1.G005000

[19] Vascik, P. D., Cho, J., Bulusu, V., and Polishchuk, V., "Geometric Approach Towards Airspace Assessment for Emerging Operations," *Journal of Air Transportation*, Vol. 28, No. 3, 2020, pp. 124–133. https://doi.org/10.2514/1.D0183

[20] Vela, A., Solak, S., Singhose, W., and Clarke, J.-P., "A Mixed Integer Program for Flight-Level Assignment and Speed Control for Conflict Resolution," *48h IEEE Conference on Decision and Control (CDC) Held Jointly with 2009 28th Chinese Control Conference*, IEEE, New York, Dec. 2009, pp. 5219–5226. https://doi.org/10.1109/CDC.2009.5400520

[21] Sripad, S., and Viswanathan, V., "The Promise of Energy-Efficient Battery-Powered Urban Aircraft," *National Academy of Sciences*, Vol. 118, No. 45, 2021, Paper e2111164118. https://doi.org/10.1073/pnas.2111164118

[22] Goyal, R., Reiche, C., Fernando, C., Serrao, J., Kimmel, S., Cohen, A., and Shaheen, S., "Urban Air Mobility Market Study," NASA Rept. HQ-E-DAA-TN65181, 2018, https://ntrs.nasa.gov/citations/20190001472 [retrieved 10 March 2022].

[23] Nathen, P., "Architectural Performance Assessment of an Electric Vertical Take-Off and Landing (e-VTOL) Aircraft Based on a Ducted Vectored Thrust Concept," April 2021, https://lilium-aviation.com/files/redaktion/refresh_feb2021/investors/Lilium_7-Seater_Paper.pdf [retrieved 10 March 2022].

[24] Silva, C., Johnson, W. R., Solis, E., Patterson, M. D., and Antcliff, K. R., "VTOL Urban Air Mobility Concept Vehicles for Technology Development," *2018 Aviation Technology, Integration, and Operations Conference*, AIAA Paper 2018-3847, June 2018. https://doi.org/10.2514/6.2018-3847

[25] Kasliwal, A., Furbush, N. J., Gawron, J. H., McBride, J. R., Wallington, T. J., DeKleine, R. D., Kim, H. C., and Keoleian, G., "Role of Flying Cars in Sustainable Mobility," *Nature Communications*, Vol. 10, No. 1, 2019, p. 1555. https://doi.org/10.1038/s41467-019-09426-0

[26] Johnson, W., and Silva, C., "NASA Concept Vehicles and the Engineering of Advanced Air Mobility Aircraft," *Aeronautical Journal*, Vol. 126, No. 1295, 2021, pp. 59–91. https://doi.org/10.1017/aer.2021.92

[27] Stoll, A. M., and Mikic, G. V., "Design Studies of Thin-Haul Commuter Aircraft with Distributed Electric Propulsion," *16th AIAA Aviation Technology, Integration, and Operations Conference*, AIAA Paper 2016-3765, June 2016. https://doi.org/10.2514/6.2016-3765

[28] White, V., "2016 Revised Value of Travel Time Guidance," 2016, https://www.transportation.gov/office-policy/transportation-policy/revised-departmental-guidance-valuation-travel-time-economic [retrieved 15 Jan. 2022].

C. Wanke
Associate Editor